

The Effect of Twisted Magnetic Field on the Period Ratio P_1/P_2 of Nonaxisymmetric MHD Waves

K. Karami^{1,2*}, K. Bahari^{3†}

¹Department of Physics, University of Kurdistan, Pasdaran Street, Sanandaj, Iran

²Research Institute for Astronomy & Astrophysics of Maragha (RIAAM), Maragha, Iran

³Physics Department, Faculty of Science, Razi University, Kermanshah, Iran

June 9, 2018

Abstract

The nonaxisymmetric magnetohydrodynamic (MHD) modes in a zero-beta cylindrical compressible thin magnetic flux tube modelled as a twisted core surrounded by a magnetically twisted annulus, both embedded in a straight ambient external field is considered. The dispersion relation is derived and solved analytically and numerically to obtain the frequencies of the nonaxisymmetric MHD waves. The main result is that the twisted magnetic annulus does affect the period ratio P_1/P_2 of the kink modes. For the kink modes, the magnetic twist in the annulus region can achieve deviations from $P_1/P_2 = 2$ of the same order of magnitude as in the observations. Furthermore, the effect of the internal twist on the fluting modes is investigated.

Subject headings: MHD — Sun: corona — Sun: magnetic fields — Sun: oscillations

*KKarami@uok.ac.ir

†K.Bahari@razi.ac.ir

1 Introduction

Transverse coronal loop oscillations triggered by explosive events, such as flares or filament eruptions, were first identified by Aschwanden et al. (1999) and Nakariakov et al. (1999) using the observations of TRACE (Transition Region And Coronal Explorer). These oscillations have been interpreted as the kink MHD modes of a cylindrical coronal flux tube by Nakariakov et al. (1999).

One of the important tools in the coronal seismology is determination of the period ratio P_1/P_2 between the period P_1 of the fundamental mode and the period P_2 of its first harmonic. The deviation of the period ratio from its canonical harmonic value of 2 has been observed in coronal loop oscillations. Verwichte et al. (2004), using the observations of TRACE, have identified the fundamental and its first harmonic of the transverse kink mode in two coronal loops. The period ratios observed by Verwichte et al. (2004) are 1.81 ± 0.25 and 1.64 ± 0.23 . However, these values were corrected with the improvement of the observational error bars to 1.82 ± 0.08 and 1.58 ± 0.06 , respectively, by Van Doorselaere, Nakariakov & Verwichte (2007). Also Verth, Erdélyi & Jess (2008) added some further corrections by considering the effects of loop expansion and estimated a period ratio of 1.54. All these values clearly are lower than 2. This may be caused by different factors such as the effects of density stratification (see e.g. Andries et al. 2005; Erdélyi & Verth 2007; Karami & Asvar 2007; Safari, Nasiri & Sobouti 2007; Karami, Nasiri & Amiri 2009) and magnetic twist (see Erdélyi & Carter 2006; Erdélyi & Fedun 2006; Karami & Barin 2009; Karami & Bahari 2010) in the loops. Note that in some cases the period ratio is shifted to higher values than 2. For instance, in Table 1 of Andries et al. (2009) there are two observational examples with $P_1/P_2 > 2$. This may be caused by the effect of magnetic field expansion (see e.g. Verth & Erdélyi 2008; Ruderman, Verth & Erdélyi 2008; Verth, Erdélyi & Jess 2008; Karami & Bahari 2011). Also there are some observational cases in which the period ratios do not show any significant departures from their canonical harmonic values. For instance, in Table 1 of Andries et al. (2009) there is an example with $P_1/P_2 = 2$. Also Van Doorselaere et al. (2009) found $P_1/P_2 \approx 2$ and $P_1/P_3 \approx 3$ in a highly twisted loop structure which is certainly not homogeneous and the loop structure could be classified as a sigmoid.

The twisted magnetic tubes have been investigated in ample detail by Bennett, Roberts & Narain (1999) and Carter & Erdélyi (2007, 2008). For a good review see Karami & Barin (2009).

Ruderman (2007) studied the nonaxisymmetric oscillations of a compressible zero-beta thin twisted magnetic tube surrounded with the straight and homogeneous magnetic field taking the density stratification into account. Using the asymptotic analysis he showed that the eigenmodes and the eigenfrequencies of the kink and the fluting oscillations are described by a classical Sturm-Liouville problem. The main result of Ruderman (2007), which also has been already obtained by Goossens, Hollweg & Sakurai (1992), was that the twist does not affect the kink mode. Note that in these analytical works, and in the present work, the azimuthal component of the equilibrium magnetic field B_ϕ is taken to be proportional to r . This is essentially because it makes the governing equations easier to solve analytically. However, this makes the equilibrium magnetic field a very particular and artificial case study and may be far from reality. It may be that more general B_ϕ equilibria do affect the kink mode.

Karami & Barin (2009) investigated both the oscillations and damping of MHD surface and hybrid waves in coronal loops in the presence of twisted magnetic field. They considered a straight cylindrical incompressible flux tube with magnetic twist just in the annulus and straight magnetic field in both the internal and external regions. They showed that the frequencies and the damping rates of both the kink and fluting modes increase when the twist parameter

increases. They obtained that the period ratio P_1/P_2 of the fundamental and first overtone for both the kink and fluting surface modes are lower than 2 (for untwisted loop) in the presence of twisted magnetic field.

Karami & Bahari (2010) examined the effect of twisted magnetic field on the resonant absorption of MHD waves in coronal loops. They concluded that with increasing the twist, the ratio of the oscillation frequency to the damping rate of the kink modes changes from 39.3 to 43.5, which approximately is one order of magnitude greater than the ratio reported by Nakariakov et al. (1999), Verwichte et al. (2004), and Wang and Solanki (2004) deduced from the TRACE data. Note that the twisted cylinder model proposed by Karami & Bahari (2010) was found produce too weak a damping rate to explain the observed strong kink wave damping.

In the present work, our main aim is to investigate the effect of twisted magnetic field on the frequencies of nonaxisymmetric MHD waves in coronal loops to justify the deviation of the period ratio P_1/P_2 from 2 observed by the TRACE. This paper is organized as follows. In Section 2 we use the asymptotic analysis obtained by Ruderman (2007) to derive the equations of motion. In Section 3 and its subsections we present the dispersion relation, two reductions to known cases, and an analytical solution. In Section 4, we give numerical results. Section 5 is devoted to conclusions.

2 Equations of motion

The linearized MHD equations for a compressible zero-beta plasma are

$$\frac{\partial \delta \mathbf{v}}{\partial t} = \frac{1}{4\pi\rho} [(\nabla \times \delta \mathbf{B}) \times \mathbf{B} + (\nabla \times \mathbf{B}) \times \delta \mathbf{B}], \quad (1)$$

$$\frac{\partial \delta \mathbf{B}}{\partial t} = \nabla \times (\delta \mathbf{v} \times \mathbf{B}), \quad (2)$$

where $\delta \mathbf{v}$ and $\delta \mathbf{B}$ are the Eulerian perturbations in the velocity and magnetic fields; ρ is the mass density.

The simplifying assumptions are as follows.

- The background magnetic field is assumed to be

$$\mathbf{B} = \begin{cases} \mathbf{B}_i = (0, A_i r, B_{zi}(r)), & r < a, \\ \mathbf{B}_0 = (0, A_0 r, B_{z0}(r)), & a < r < R, \\ \mathbf{B}_e = (0, 0, B_{ze}), & r > R, \end{cases} \quad (3)$$

where A_i , A_0 , B_{ze} are constant and a , R are radii of the core and the tube, respectively.

From both the equilibrium equation, i.e. $\frac{dB^2}{dr} = -\frac{2B_\phi^2}{r}$, and the continuity condition of the magnetic pressure across the boundaries of the tube, i.e. $B_i^2(a) = B_0^2(a)$, $B_0^2(R) = B_e^2(R)$, the z -component of the equilibrium magnetic field can be obtained as

$$\begin{aligned} B_{zi}^2(r) &= B_0^2 + A_i^2(a^2 - 2r^2), \\ B_{z0}^2(r) &= B_0^2 + A_0^2(a^2 - 2r^2), \\ B_{ze}^2 &= B_0^2 + A_0^2(a^2 - R^2), \end{aligned} \quad (4)$$

where B_0 is an integration constant. The above magnetic field configuration in the absence of the annulus is the same as the background magnetic field considered by Ruderman (2007).

- ρ is constant along the loop but different in the interior, annulus and exterior regions and denoted by ρ_i , ρ_0 and ρ_e , respectively.
- We consider the flux tube to be a cylinder and therefore implement the cylindrical coordinates, (r, ϕ, z) .
- The plasma equilibrium is fixed to be in a steady state, i.e., without flow.
- t -, ϕ - and z -dependence for any of the components $\delta\mathbf{v}$ and $\delta\mathbf{B}$ is $\exp\{i(m\phi + k_z z - \omega t)\}$. Here $k_z = l\pi/L$ and L is the tube length. Also l and m are the longitudinal and azimuthal mode numbers, respectively.

Here like Ruderman (2007) we consider $\epsilon := \frac{Aa}{B_0} \sim k_z a \ll 1$ which is in good agreement with the observations and also look for the low frequency eigenmodes. Following the second order perturbation method in terms of ϵ given by Ruderman (2007), solutions of Eqs. (1)-(2) in terms of $\delta P = \frac{\mathbf{B} \cdot \delta\mathbf{B}}{4\pi}$, the Eulerian perturbation in the magnetic pressure, and $\xi_r = -\delta v_r / i\omega$, the Lagrangian perturbation in the radial displacement, for the interior and annulus regions yield

$$\delta P(r) = \frac{r}{m^2} \left(\rho\omega^2 - \frac{B_0^2}{4\pi} F^2 \right) \frac{d(r\xi_r)}{dr} + \left(\frac{B_0 A F}{2\pi m} \right) r \xi_r, \quad (5)$$

$$\frac{d}{dr} \left(r \frac{d(r\xi_r)}{dr} \right) - m^2 \xi_r = 0, \quad (6)$$

where $F = k_z + m \frac{A}{B_0}$. Equations (5) and (6) are same as Eqs. (19) and (21), respectively, in Ruderman (2007).

In the interior and annulus regions, solutions of Eq. (6) are

$$\xi_r(r) = \begin{cases} \alpha r^{m-1}, & r < a, \\ \beta r^{m-1} + \gamma r^{-m-1}, & a < r < R, \end{cases} \quad (7)$$

and solutions for $\delta P(r)$ are obtained from substituting Eq. (7) in (5) as

$$\delta P(r) = \left(\rho_i \omega^2 - \frac{B_0^2 F_i^2}{4\pi} + \frac{B_0 A_i F_i}{2\pi} \right) \frac{\alpha r^m}{m}, \quad r < a, \quad (8)$$

$$\begin{aligned} \delta P(r) &= \left(\rho_0 \omega^2 - \frac{B_0^2 F_0^2}{4\pi} + \frac{B_0 A_0 F_0}{2\pi} \right) \frac{\beta r^m}{m} \\ &\quad - \left(\rho_0 \omega^2 - \frac{B_0^2 F_0^2}{4\pi} - \frac{B_0 A_0 F_0}{2\pi} \right) \frac{\gamma r^{-m}}{m}, \quad a < r < R. \end{aligned} \quad (9)$$

For the exterior region, $r > R$, we obtain

$$\frac{d^2 \delta P}{dr^2} + \frac{1}{r} \frac{d\delta P}{dr} - \left(k'^2 + \frac{m^2}{r^2} \right) \delta P = 0, \quad (10)$$

$$\xi_r(r) = -\frac{4\pi}{k'^2 B_0^2} \frac{d\delta P}{dr}, \quad (11)$$

where

$$k'^2 = k_z^2 - \frac{4\pi\rho_e\omega^2}{B_0^2}. \quad (12)$$

Equations (10) and (11) are same as Eqs. (26) and (25a), respectively, in Ruderman (2007). In the exterior region, $r > R$, the waves should be evanescent. Solutions are

$$\delta P(r) = \varepsilon K_m(k'r), \quad k'^2 > 0, \quad (13)$$

$$\xi_r(r) = -\varepsilon \frac{4\pi}{k'B_0^2} K'_m(k'r), \quad (14)$$

where K_m is the modified Bessel function of the second kind and a prime on K_m indicates a derivative with respect to its appropriate argument. The coefficients α, β, γ and ε in Eqs. (7), (8), (9), (13) and (14) are determined by the appropriate boundary conditions.

3 Boundary conditions and dispersion relation

The necessary boundary conditions at the perturbed tube boundary are that the plasma displacement in the radial direction and the magnetic pressure should be continuous as

$$\xi_{ri}\Big|_{r=a} = \xi_{r0}\Big|_{r=a}, \quad \xi_{r0}\Big|_{r=R} = \xi_{re}\Big|_{r=R}, \quad (15)$$

$$\begin{aligned} \delta P_1 - \frac{B_{\phi i}^2}{4\pi a} \xi_{ri}\Big|_{r=a} &= \delta P_0 - \frac{B_{\phi 0}^2}{4\pi a} \xi_{r0}\Big|_{r=a}, \\ \delta P_0 - \frac{B_{\phi 0}^2}{4\pi R} \xi_{r0}\Big|_{r=R} &= \delta P_e\Big|_{r=R}. \end{aligned} \quad (16)$$

Using the above boundary conditions and the solutions given by Eqs. (7), (8), (9) for the internal and annulus regions and Eqs. (13), (14) for the exterior region, the dispersion relation is derived as

$$\begin{aligned} & \left(\Xi_m^0 \Pi_m^0 - \Xi_m^i \Xi_m^e \right) \left[1 - (a/R)^{2m} \right] \\ & - \Xi_m^i \left[\Xi_m^0 - (a/R)^{2m} \Pi_m^0 \right] \\ & + \Xi_m^e \left[\Pi_m^0 - (a/R)^{2m} \Xi_m^0 \right] = 0, \end{aligned} \quad (17)$$

with

$$\begin{aligned} \Xi_m^j &= \frac{1}{m} \left(\rho_j \omega^2 - \frac{B_0^2 k_z^2}{4\pi} \right) \\ & + \frac{A_j}{4\pi m} (2B_0 k_z + mA_j)(1 - m), \end{aligned} \quad (18)$$

$$\begin{aligned} \Pi_m^0 &= -\frac{1}{m} \left(\rho_0 \omega^2 - \frac{B_0^2 k_z^2}{4\pi} \right) \\ & + \frac{A_0}{4\pi m} (2B_0 k_z + mA_0)(1 + m), \end{aligned} \quad (19)$$

$$\Xi_m^e = \frac{B_0^2}{4\pi} \frac{k'^2}{k'R} \frac{K_m(k'R)}{K'_m(k'R)}, \quad (20)$$

where the superscript j in Ξ_m^j stands for i and 0 corresponding to the interior and annulus regions, respectively.

Note that if we remove the annulus region by setting $a = R$ in the dispersion relation (17) and using the thin flux tube approximation for $K_m(x) \propto x^{-m}$ at small x , the result yields

$$\omega^2 = C_k^2 \left\{ k_z^2 + \frac{A_i(m-1)}{2B_0^2} (2B_0 k_z + A_i m) \right\}, \quad (21)$$

where $C_k^2 = \frac{B_0^2}{2\pi(\rho_i + \rho_e)}$. Equation (21) is same as Eq. (40) in Ruderman (2007). The main result of Ruderman (2007) is that the twist does not affect the kink modes in the particular case of having $B_\phi \propto r$ and Eq. (21) shows that we get the same frequencies as in the case that $A_i = 0$. This result also has been already obtained by Goossens, Hollweg & Sakurai (1992). Note that Eq. (17) shows that even in the presence of annulus, the internal twist does not affect the kink ($m = 1$) modes. Because the internal twist, A_i , only appears in Eq. (18) and when $m = 1$ then it has no contribution.

In subsections 3.1 and 3.2, we show that the dispersion relation (17) for the cases $A_i = 0$ and $A_0 = 0$, respectively, reduces to two known cases. Also in subsection 3.3, we give an analytical solution for the dispersion relation (17).

3.1 Case $A_i = 0$

Here we show that the dispersion relation (17) in the absence of internal twist, i.e. $A_i = 0$, can be obtained from the dispersion relation, Eq. (6b), given by Carter & Erdélyi (2008) under the thin tube (TT) approximation (or long-wavelength limit), i.e. $k_z a \ll 1$. The dispersion relation Eq. (6b) in Carter & Erdélyi (2008) for body waves has the form

$$\frac{\Xi_{aY} - \Xi_i + \Xi_{aY} \Xi_i \frac{A_0^2}{4\pi} Y_m(n_0 a)}{\Xi_{aJ} - \Xi_i + \Xi_{aJ} \Xi_i \frac{A_0^2}{4\pi} J_m(n_0 a)} = \frac{Y_m(n_0 R) \Xi_{RY} - \Xi_e + \Xi_{RY} \Xi_e \frac{A_0^2}{4\pi}}{J_m(n_0 R) \Xi_{RJ} - \Xi_e + \Xi_{RJ} \Xi_e \frac{A_0^2}{4\pi}}, \quad (22)$$

which is valid for thick magnetic tubes with twisted annulus in the incompressible limit. Note that according to Edwin & Roberts (1983) there are no surface waves in zero-beta approximation which is compatible with coronal conditions. Although the plasma in our model is compressible, the results concerning the kink ($m = 1$) modes for incompressible plasmas given by Carter & Erdélyi (2008) can be applied to coronal loops despite that the coronal plasma is a low-beta plasma (see Carter & Erdélyi 2007; Erdélyi & Fedun 2007). Recently, Goossens et al. (2009) showed that in the TT approximation neglecting contributions proportional to $(k_z a)^2$ then the frequencies of the kink wave are the same in the three cases including a compressible pressureless plasma, an incompressible plasma and a compressible plasma which allows for MHD radiation.

Under the TT approximation, we have

$$\frac{xK'_m(x)}{K_m(x)} = \frac{xY'_m(x)}{Y_m(x)} = -m + O(x^2), \quad (23)$$

$$\frac{xI'_m(x)}{I_m(x)} = \frac{xJ'_m(x)}{J_m(x)} = m + O(x^2), \quad (24)$$

where (J_m, Y_m) and (I_m, K_m) are the Bessel and modified Bessel functions of the first and second kind, respectively. Using Eqs. (23), (24), the different terms appeared in Eq. (22) given by Carter & Erdélyi (2008) reduce to

$$\Xi_{aY} = \Xi_{RY} = -\frac{m}{\rho_0} \frac{1}{(\omega^2 - \omega_{A_0}^2) - \frac{2A_0\omega_{A_0}}{\sqrt{4\pi\rho_0}}}, \quad (25)$$

$$\Xi_{aJ} = \Xi_{RJ} = \frac{m}{\rho_0} \frac{1}{(\omega^2 - \omega_{A_0}^2) + \frac{2A_0\omega_{A_0}}{\sqrt{4\pi\rho_0}}}, \quad (26)$$

$$\Xi_i = \frac{m}{\rho_i(\omega^2 - \omega_{A_i}^2)}, \quad (27)$$

$$\Xi_e = \frac{-m}{\rho_e(\omega^2 - \omega_{A_e}^2)}, \quad (28)$$

where following Carter & Erdélyi (2008), ω_{A_0} , ω_{A_i} , and ω_{A_e} are the Alfvén frequencies in the annulus, internal and external regions, respectively, given by

$$\omega_{A_0} = \frac{1}{\sqrt{4\pi\rho_0}}(mA_0 + k_z B_0), \quad (29)$$

$$\omega_{A_i} = \frac{k_z B_i}{\sqrt{4\pi\rho_i}}, \quad (30)$$

$$\omega_{A_e} = \frac{k_z B_e}{\sqrt{4\pi\rho_e}}. \quad (31)$$

Using Eqs. (18) to (20) and Eqs. (23) to (31), one can rewrite the terms $\Xi_Y := \Xi_{aY} = \Xi_{RY}$, $\Xi_J := \Xi_{aJ} = \Xi_{RJ}$, Ξ_i , and Ξ_e appeared in the dispersion relation (22) as follows

$$\Xi_i = \frac{1}{\Xi_m^i}, \quad (32)$$

$$\Xi_J = \frac{1}{\Xi_m^0 + \frac{A_0^2}{4\pi}}, \quad (33)$$

$$\Xi_Y = \frac{1}{\Pi_m^0 + \frac{A_0^2}{4\pi}}, \quad (34)$$

$$\Xi_e = \frac{4\pi m}{B_0^2 k'^2} = -\frac{1}{\Xi_m^e}. \quad (35)$$

Also under the TT approximation we have

$$\frac{Y_m(n_0 R)}{Y_m(n_0 a)} \frac{J_m(n_0 a)}{J_m(n_0 R)} = \left(\frac{a}{R}\right)^{2m}. \quad (36)$$

One can easily show that substituting Eqs. (32) to (36) into (22) yields

$$R^{2m} \frac{\Xi_m^0 + \Xi_m^e}{\Pi_m^0 + \Xi_m^e} = a^{2m} \frac{\Xi_m^0 - \Xi_m^i}{\Pi_m^0 - \Xi_m^i}, \quad (37)$$

which is nothing but Eq. (17) in which the terms a^{2m} and R^{2m} have been grouped.

3.2 Case $A_0 = 0$

Here we present that the dispersion relation (37) in the absence of twist in the annulus region, i.e. $A_0 = 0$, is same as the dispersion relation Eq. (11) in Carter & Erdélyi (2007) for the kink ($m = 1$) modes in the TT approximation. By setting $A_0 = 0$, Eqs. (18) to (20) reduce to

$$\Xi_1^i = \rho_i(\omega^2 - \omega_{A_i}^2), \quad (38)$$

$$\Xi_1^0 = \rho_0(\omega^2 - \omega_{A_{0z}}^2), \quad (39)$$

$$\Pi_1^0 = -\rho_0(\omega^2 - \omega_{A_{0z}}^2), \quad (40)$$

$$\Xi_1^e = \rho_e(\omega^2 - \omega_{A_e}^2), \quad (41)$$

where

$$\omega_{A_{0z}} = \frac{k_z B_0}{\sqrt{4\pi\rho_0}}. \quad (42)$$

With the help of above expressions, Eq. (37) yields

$$\frac{Q_0^i + 1}{Q_0^i - 1} - \left(\frac{a}{R}\right)^2 \frac{Q_0^e - 1}{Q_0^e + 1} = 0, \quad (43)$$

where

$$Q_0^i = \frac{\rho_i}{\rho_0} \left(\frac{\omega^2 - \omega_{A_i}^2}{\omega^2 - \omega_{A_{0z}}^2} \right), \quad (44)$$

$$Q_0^e = \frac{\rho_e}{\rho_0} \left(\frac{\omega^2 - \omega_{A_e}^2}{\omega^2 - \omega_{A_{0z}}^2} \right). \quad (45)$$

Equation (43) is same as the dispersion relation (11) in Carter & Erdélyi (2007) for the kink ($m = 1$) modes in the TT approximation.

3.3 Analytical solution of the dispersion relation

Here we try to solve the dispersion relation (17), analytically. To do this we apply the TT approximation, Eq. (23), to the expression Ξ_m^e , Eq. (20). This reduces the dispersion relation (17) to a second order equation in terms of ω^2 which can now be solved analytically. To write the solutions in a simple form, we define two expressions X_m^j and Z_m^0 as follows

$$X_m^j = \frac{A_j}{B_0 k_z} \left(2 + \frac{mA_j}{B_0 k_z} \right) (1 - m), \quad (46)$$

$$Z_m^0 = \frac{A_0}{B_0 k_z} \left(2 + \frac{mA_0}{B_0 k_z} \right) (1 + m), \quad (47)$$

which are proportional to the second terms appeared in Eqs. (18) and (19), respectively. These expressions contain all twist parameters in the dispersion relation.

Using Eqs. (46) and (47), one can rewrite Eq. (17) as

$$c_m \left(\frac{\sqrt{4\pi\rho_i}}{B_0 k_z} \right)^4 \omega^4 - c_{ml} \left(\frac{\sqrt{4\pi\rho_i}}{B_0 k_z} \right)^2 \omega^2 + \tilde{c}_{ml} = 0, \quad (48)$$

where c_m , c_{ml} and \tilde{c}_{ml} are constants defined as

$$c_m = \left[\frac{\rho_e}{\rho_i} + \left(\frac{\rho_0}{\rho_i} \right)^2 \right] \left(1 - (a/R)^{2m} \right) + \frac{\rho_0}{\rho_i} \left(1 + \frac{\rho_e}{\rho_i} \right) \left(1 + (a/R)^{2m} \right), \quad (49)$$

$$c_{ml} = 2 \left(1 + \frac{\rho_e}{\rho_i} + 2 \frac{\rho_0}{\rho_i} \right) + \left[\frac{\rho_0}{\rho_i} + \frac{\rho_e}{\rho_i} + \left(1 - \frac{\rho_0}{\rho_i} \right) (a/R)^{2m} \right] Z_m^0 - \left[1 + \frac{\rho_0}{\rho_i} + \left(\frac{\rho_e}{\rho_i} - \frac{\rho_0}{\rho_i} \right) (a/R)^{2m} \right] X_m^0 - \left[\frac{\rho_0}{\rho_i} + \frac{\rho_e}{\rho_i} + \left(\frac{\rho_0}{\rho_i} - \frac{\rho_e}{\rho_i} \right) (a/R)^{2m} \right] X_m^i, \quad (50)$$

$$\tilde{c}_{ml} = 4 - 2 \left(X_m^i + X_m^0 - Z_m^0 \right) - \left(Z_m^0 - X_m^i \right) X_m^0 - (a/R)^{2m} \left(X_m^i - X_m^0 \right) Z_m^0. \quad (51)$$

Here c_m depends only on the azimuthal mode number m but c_{ml} and \tilde{c}_{ml} contain both the azimuthal m and longitudinal l mode numbers. Note that l appears in $k_z = l\pi/L$.

Now solving Eq. (48) gives the eigenfrequencies

$$\omega_{nml} = \frac{k_z B_0}{\sqrt{4\pi\rho_i}} \left(\frac{c_{ml} \pm \sqrt{c_{ml}^2 - 4\tilde{c}_{ml}c_m}}{2c_m} \right)^{1/2}, \quad (52)$$

where the subscript n (or \pm signs) denotes the radial mode number corresponding to the lower ($n = 1$) and upper ($n = 2$) frequencies of the two nonaxisymmetric modes. Note that for kink ($m = 1$) modes from Eq. (46) we get $X_m^i = X_m^0 = 0$. Also from Eqs. (50) and (51) for $m = 1$ both c_{ml} and \tilde{c}_{ml} are positive. On the other hand c_m is always positive. Therefore, from Eq. (52) the $-$ and $+$ signs are corresponding to the radial mode numbers $n = 1$ and $n = 2$, respectively. Since our model is based on the TT approximation, the numerical solution of the dispersion relation (17) in Section 4 is approximately same as the analytical solution (52).

Note that in addition to the solutions (52), there is a set of broadband body modes which has been already predicted by Carter & Erdélyi (2008). However, these modes are lost from the solutions of the dispersion relation (22) under the TT approximation. Since our model is based on the TT approximation, therefore the infinite set of body modes are absent in our calculations. In accordance with the classification introduced by Roberts (1981), the modes both described and not described by Eq. (17) are body waves in the zero-beta plasma approximation. To distinguish the kink mode described by Eq. (17) from those not described by Eq. (17), Ruderman and Roberts (2002) suggested calling the solutions (52) “global kink modes,” retaining the name “body kink modes” for all other kink modes. We generalize this convention for fluting modes and call fluting modes described by Eq. (17) “global fluting modes,” retaining the name “body fluting modes” for all other fluting modes.

4 Numerical results

To solve the dispersion relation (17), numerically, we choose the physical parameters $L = 10^5$ km, $a/L = 0.01$, $\rho_e/\rho_i = 0.1$, $\rho_0/\rho_i = 0.5$, $\rho_i = 2 \times 10^{-14}$ g cm $^{-3}$, $B_0 = 100$ G. For such a loop one finds $v_{A_i} = \frac{B_0}{\sqrt{4\pi\rho_i}} = 2000$ km s $^{-1}$, $\omega_{A_i} := \frac{v_{A_i}}{L} = 0.02$ rad s $^{-1}$. In what follows, we illustrate our numerical studies in the two separate equilibrium cases where there is (i) Twist in both the core and annulus regions (ii) Twist in the core and no twist in the annulus.

4.1 Case $A_i \neq 0$ and $A_0 \neq 0$

The effect of twisted magnetic field on the frequencies ω is calculated by the numerical solution of the dispersion relation, Eq. (17). Figures 1 to 2 show the frequencies of the fundamental and first overtone $l = 1, 2$ kink ($m = 1$) modes with radial mode numbers $n = 1, 2$ versus the twist parameter of the annulus, $B_\phi/B_z := \frac{A_0 a}{B_0}$, and for different relative core widths $a/R =$

(0.65, 0.9, 0.99). Note that here the parameter A_i does not need to be set explicitly. Because the second term in Eq. (18) containing the contribution of the parameter A_i is automatically removed for the kink ($m = 1$) modes.

Figures 1 to 2 reveal that: i) for a given a/R , the frequencies increase when the twist parameter of the annulus increases. The result is in good agreement with that obtained by Carter & Erdélyi (2008) and Karami & Barin (2009). ii) For a given n and a/R , when the longitudinal mode number, l , increases, the frequencies increase. iii) For a given l , a/R and B_ϕ/B_z , when the radial mode number, n , increases, the frequencies increase. iv) For $n = 1$, when a/R goes to unity then the frequencies become independent of B_ϕ/B_z . Therefore in the absence of the annulus, the twist does not affect the kink modes in the specific case of having $B_\phi \propto r$. This is in good agreement with that obtained by Goossens, Hollweg & Sakurai (1992) and Ruderman (2007). v) For $n = 2$, when a/R goes to unity exactly then the second mode is removed. This is expected to be occurred because for $a/R = 1$ we have only one boundary in the tube corresponding to one mode.

To compare our results with those of Carter & Erdélyi (2008), we use Eq. (22) and obtain the frequencies of the kink ($m = 1$) modes with radial mode number ($n = 2$) versus the twist parameter of the annulus and for different values of $k_z a = \pi a/L = (\pi/100, 0.1, 1)$. The results are displayed in Fig. 3. The result for $k_z a = 1$ has been already obtained by Carter & Erdélyi (2008) for incompressible flux tube with twisted annulus. Figure 3 shows that for a slender tube with $k_z a = \pi/100$ there is a much greater variation with the twist in the annulus than what Carter & Erdélyi (2008) found for thicker tube with $k_z a = 1$.

One important problem about the frequencies displayed in Figs. 1 and 2 is that in all four panels in these figures, all the curves for different values of a/R intersect at a single point. For instance, in Fig. 1 for the fundamental and first overtone kink modes, the frequencies of the intersection points are $\omega_{111} = 4.23$ and $\omega_{112} = 2\omega_{111} = 8.46$, respectively. Also the location of the intersection point for the fundamental kink mode ω_{111} occurs at $B_\phi/B_z = \frac{A_0 a}{B_0} = 0.0055$ and for the first overtone kink mode ω_{112} the intersection occurs exactly at twice the value as for the fundamental mode. The frequency and the twist of the intersection point can be obtained from the dispersion relation. To do this we rewrite the dispersion relation (37) for the kink ($m = 1$) modes as

$$f - \left(\frac{a}{R}\right)^2 g = 0, \quad (53)$$

where

$$f = \frac{\Pi_1^0 - \Xi_1^i}{\Xi_1^0 - \Xi_1^i}, \quad (54)$$

$$g = \frac{\Pi_1^0 + \Xi_1^e}{\Xi_1^0 + \Xi_1^e}. \quad (55)$$

If we set $f = g = 0$, then the result of the dispersion relation (53) would be independent of the term a/R . Therefore the set of equations $\Pi_1^0 - \Xi_1^i = 0$ and $\Pi_1^0 + \Xi_1^e = 0$ by the help of Eqs. (18) to (20) in the TT approximation yield

$$\omega = C_k k_z = \frac{B_0}{\sqrt{2\pi(\rho_i + \rho_e)}} \frac{l\pi}{L}, \quad (56)$$

$$\frac{B_\phi}{B_z} = \frac{A_0 a}{B_0} = \left(\sqrt{\frac{\rho_i + \rho_0}{\rho_i + \rho_e}} - 1 \right) \frac{l\pi a}{L}, \quad (57)$$

which show that the values of both the frequency and the twist of the intersection point depend on the wavelength as observed. Taking $L = 10^5$ km, $a/L = 0.01$, $\rho_e/\rho_i = 0.1$, $\rho_0/\rho_i = 0.5$, and

$B_0 = 100$ G, then Eqs. (56) and (57) give $\omega/\omega_{A_i} = 4.24 l$ and $B_\phi/B_z = \frac{A_0 a}{B_0} = 0.0053 l$ which are in good agreement with the numerical results obtained for the frequency and the twist of the intersection point in Fig. 1.

To investigate this problem from another point of view, the radial component of the fundamental kink eigenfunctions, $\xi_r(r)$, is studied. To do this, using the eigenfrequencies obtained from the dispersion relation (17) and applying the boundary conditions (15) and (16) to the solutions (7), (8), (9), (13) and (14) one can obtain the coefficients α , β , γ and ε . Then with the help of Eqs. (7) and (14) the radial component of the fundamental kink eigenfunctions $\xi_r(r)$ can be obtained. The results of $\xi_r(r)$ for different relative core widths $a/R = (0.65, 0.9, 0.99)$ and for two different values of the twist parameter of the annulus $B_\phi/B_z = \frac{A_0 a}{B_0} = 0.0055$ and 0.02 are plotted in Figs. 4 and 5, respectively. Note that the intersection occurs at $B_\phi/B_z = 0.0055$. Comparing Fig. 4 with 5 we find out for the twist parameter of the annulus 0.0055 , the eigenfunctions at the second boundary behave smoothly. This means that at the intersection point, the location of the second boundary is not important or physically the variation of the thickness of the annulus does not affect the eigenfunctions or eigenfrequencies. Figure 5 clears that for the twist parameter of the annulus 0.02 where the intersection does not occur, the behavior of the eigenfunctions depends on the thickness of the annulus region.

To compare the kink oscillations for different radial mode numbers n , the radial component of the kink eigenfunctions with $n = 2$ is plotted in Fig. 6 for the twist parameter of the annulus $B_\phi/B_z = \frac{A_0 a}{B_0} = 0.02$ and for different relative core widths $a/R = (0.65, 0.9, 0.99)$. **Figure 6 shows that contrary to the $n = 1$ mode in which the core and annulus regions oscillate with the same phase (see Fig. 5), for $n = 2$ the kink oscillations of the core and annulus region, having opposite signs of $\xi_r(r)$, are out of phase with each other. This is in agreement with the previous results obtained by Mikhlyayev & Solov'ev (2005) and Ruderman & Erdélyi (2009).**

The period ratio P_1/P_2 of the fundamental and first overtone, $l = 1, 2$ modes of the kink ($m = 1$) waves with $n = 1, 2$ versus the twist parameter of the annulus are plotted in Figs. 7 to 8. Figures 7 to 8 show that: i) the period ratio P_1/P_2 with increasing the twist parameter of the annulus, for $n = 1$ decreases from 2 (for untwisted loop), comes down to a minimum and then increases. Whereas for $n = 2$, it decreases from 2 and approaches below 1.6 for $a/R = 0.5$, for instance. Note that when the twist is zero, the diagrams of P_1/P_2 do not start exactly from 2. This may be caused by the radial structuring ($\rho_0 \neq \rho_i$, $\rho_e \neq \rho_i$). But for the selected thin tube with $a/L = 0.01$, this departure is very small, $O(10^{-4})$, and doesn't show itself in the diagrams (see McEwan et al. 2006). ii) For a given B_ϕ/B_z , the period ratio P_1/P_2 for $n = 1$ increases and for $n = 2$ decreases when the relative core width increases. Figure 7 clears that for the kink modes ($m = 1, n = 1$) with $a/R = 0.5$, for both $B_\phi/B_z = 0.0107$ and 0.0153 the ratio P_1/P_2 is 1.82. This is in good agreement with the period ratio observed by Van Doorsselaere, Nakariakov & Verwichte (2007), 1.82 ± 0.08 , deduced from the observations of TRACE. See also McEwan, Díaz & Roberts (2008). For more observational examples of the period ratio, we estimate the twist parameter of the annulus for the kink modes ($m = 1, n = 1$) with different relative core widths. The results which can give the same P_1/P_2 observed by the TRACE are summarized in Table 1.

Note that the results of Fig. 7 and Table 1 show that the period ratio P_1/P_2 of the kink ($m = 1$) modes for $n = 1$ is not a monotonic function of the twist parameter of the annulus. The analytical solution (52) also confirms this behavior. Therefore, we conclude that the value of the twist parameter in coronal loops cannot be determined uniquely using the model studied here.

Finally, it is worth to say some remarks regarding the coronal seismology using the period

ratio P_1/P_2 of the kink ($m = 1$) modes. Although the kink modes with $n = 1$ and $n = 2$ can be excited in the flux tube, to compare the results with the observation, we considered only the period ratio P_1/P_2 of the fundamental ($l = 1$) and its first overtone ($l = 2$) kink ($m = 1$) modes with $n = 1$. Because as we already mentioned in the case $n = 2$ the core and annulus oscillate with the opposite phases. This yields small transverse global displacement for the tube which is not compatible with the observed displacements of coronal loops, roughly 20 Mm from the loop top (see Verwichte et al. 2004). The other possibility for explaining the observed P_1/P_2 is the longitudinal fundamental ($l = 1$) kink modes of $n = 1$ and $n = 2$. But this case also cannot justify the observations. Following Verwichte et al. 2004, the long-period oscillation is the fundamental mode, with a maximum amplitude at the loop top. The short period oscillation is its second harmonic. It has a node at the loop top, i.e. $l = 2$. One notes that besides the two global kink modes with $n = 1, 2$, an infinite set of body kink modes can also be excited in the tube. However, the body modes due to having oscillatory displacements inside the tube cannot drive the loop to oscillate globally.

4.2 Case $A_i \neq 0$ and $A_0 = 0$

As we mentioned before, the internal twist does not affect the kink ($m = 1$) modes. Hence, we extend our investigation to the fluting ($m = 2$) modes and study the effect of internal twist on their frequencies by the numerical solution of the dispersion relation, Eq. (17), in the absence of twist in the annulus region. Figure 9 shows the frequencies of the fundamental and first overtone $l = 1, 2$ fluting ($m = 2$) modes with radial mode number $n = 1$ versus the internal twist parameter, $B_\phi/B_z := \frac{A_i a}{B_0}$, when $A_0 = 0$ and for different relative core widths $a/R = (0.65, 0.9, 0.99)$. Figure 9 clears that: i) for a given a/R , the frequencies increase when the internal twist parameter increases. ii) For a given a/R , when the longitudinal mode number, l , increases, the frequencies increase. iii) When a/R goes to unity then the frequencies obey Eq. (21).

Figure 10 shows the period ratio P_1/P_2 of the fundamental and first overtone, $l = 1, 2$ modes of the fluting ($m = 2$) waves with $n = 1$ versus the internal twist parameter when $A_0 = 0$. Figure 10 presents that: i) the period ratio P_1/P_2 with increasing the internal twist parameter, decreases from 2 (for untwisted loop) and approaches below 1.6 for $a/R = 0.5$, for instance. ii) For a given B_ϕ/B_z , the period ratio P_1/P_2 decreases when the relative core width increases.

5 Conclusions

Oscillations of nonaxisymmetric MHD waves in coronal loops in the presence of the twisted magnetic field is studied. To do this, a coronal loop is considered as a straight cylindrical compressible zero-beta thin flux tube with magnetic twist in the internal and the annulus and straight magnetic field in the external region. Using the perturbation method given by Ruderman (2007), the dispersion relation is obtained and solved both analytically and numerically for obtaining the frequencies of the nonaxisymmetric modes. Our dispersion relation confirms the results of other people for the different cases. For instance: i) it shows that in the absence of annulus region, the twist does not affect the kink ($m = 1$) modes which is same as the result obtained by Goossens, Hollweg & Sakurai (1992) and Ruderman (2007). ii) In the absence of internal twist, the dispersion relation reduces to the same result derived by Carter & Erdélyi (2008) in the TT approximation. iii) In the absence of twist in the annulus region, the dispersion relation yields the same result obtained by Carter & Erdélyi (2007) for the kink ($m = 1$) modes

in the TT approximation. Furthermore, the effect of the internal twist on the fluting ($m = 2$) modes is investigated. Our numerical results show that

i) for a given relative core width, frequencies of the fundamental and first overtone $l = 1, 2$ kink ($m = 1$) modes with radial mode numbers $n = 1, 2$ increase when the twist parameter of the annulus increases. The same behavior holds for the frequencies of the fluting ($m = 2$) modes with $n = 1$ when the internal twist parameter increases;

ii) when the relative core width, a/R , goes to unity then the kink ($m = 1$) modes with $n = 1$ become independent of the twist and in the case of $a/R = 1$ the second mode labeled by $n = 2$ is removed from the system;

iii) the period ratio P_1/P_2 for the kink ($m = 1$) modes with $n = 1, 2$ is lower than 2 (for untwisted loop) in the presence of the twisted magnetic annulus. The results of P_1/P_2 for the kink ($m = 1$) modes with $n = 1$ are in accordance with some observations of the TRACE. The period ratio for the fluting ($m = 2$) modes with $n = 1$ decreases from 2 with increasing the internal twist parameter.

Acknowledgements

The authors thank the anonymous referee for a number of valuable suggestions. The work of K. Karami has been supported financially by Research Institute for Astronomy and Astrophysics of Maragha (RIAAAM) under research project No. 1/1551.

References

- [1] Andries, J., Goossens, M., Hollweg, J.V., Arregui, I., Van Doorselaere, T., 2005. A&A 430, 1109.
- [2] Andries, J., Van Doorselaere, T., Roberts, B., Verth, G., Verwichte, E., Erdélyi, R., 2009. Space Sci. Rev. 149, 3.
- [3] Aschwanden, M.J., Fletcher, L., Schrijver, C.J., Alexander, D., 1999. ApJ 520, 880.
- [4] Ballai, I., Jess, D.B., Douglas, M., 2011. A&A 534, A13.
- [5] Bennett, K., Roberts, B., Narain, U., 1999. Sol. Phys. 185, 41.
- [6] Carter, B.K., Erdélyi, R., 2007. A&A 475, 323.
- [7] Carter, B.K., Erdélyi, R., 2008. A&A 481, 239.
- [8] Edwin, P.M., Roberts, B., 1983. Sol. Phys. 88, 179.
- [9] Erdélyi, R., Carter, B.K., 2006. A&A 455, 361.
- [10] Erdélyi, R., Fedun, V., 2006. Sol. Phys. 238, 41.
- [11] Erdélyi, R., Fedun, V., 2007. Sol. Phys. 246, 101.
- [12] Erdélyi, R., Verth, G., 2007. A&A 462, 743.
- [13] Goossens, M., Hollweg, J.V., Sakurai, T., 1992. Sol. Phys. 138, 233.
- [14] Goossens, M., Terradas, J., Andries, J., Arregui, I., Ballester, J.L., 2009. A&A 503, 213.

- [15] Karami, K., Asvar, A., 2007. MNRAS 381, 97.
- [16] Karami, K., Barin, M., 2009. MNRAS 394, 521.
- [17] Karami, K., Nasiri, S., Amiri, S., 2009. MNRAS 394, 1973.
- [18] Karami, K., Bahari, K., 2010. Sol. Phys. 263, 87.
- [19] Karami, K., Bahari, K., 2011. Ap&SS 333, 463.
- [20] McEwan, M.P., Donnelly, G.R., Díaz, A.J., Roberts, B., 2006. A&A 460, 893.
- [21] McEwan, M.P., Díaz, A.J., Roberts, B., 2008. A&A 481, 819.
- [22] Mikhalyaev, B.B., Solov'ev, A.A., 2005. Sol. Phys. 227, 249.
- [23] Nakariakov, V.M., Ofman, L., DeLuca, E.E., Roberts, B., Davila, J.M., 1999. Science 285, 862.
- [24] Roberts, B., 1981. Sol. Phys. 69, 27.
- [25] Ruderman, M.S., 2007. Sol. Phys. 246, 119.
- [26] Ruderman, M.S., Erdélyi, R., 2009. Space Sci. Rev. 149, 199.
- [27] Ruderman, M.S., Roberts, B., 2002. ApJ 577, 475.
- [28] Ruderman, M.S., Verth, G., Erdélyi, R., 2008. ApJ 686, 694.
- [29] Safari, H., Nasiri, S., Sobouti, Y., 2007. A&A 470, 1111.
- [30] Van Doorselaere, T., Nakariakov, V.M., Verwichte, E., 2007. A&A 473, 959.
- [31] Van Doorselaere, T., Birtill, D.C.C., Evans, G.R., 2009. A&A 508, 1485.
- [32] Verth, G., Erdélyi, R., 2008. A&A 486, 1015.
- [33] Verth, G., Erdélyi, R., Jess, D.B., 2008. ApJ 687, L45.
- [34] Verwichte, E., Nakariakov, V.M., Ofman, L., Deluca, E.E., 2004. Sol. Phys. 223, 77.
- [35] Wang, T.J., Solanki, S.K., 2004. A&A 421, L33.

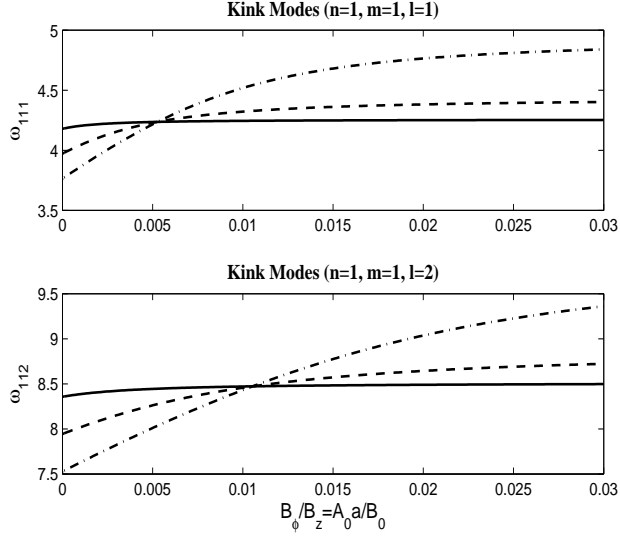


Figure 1: Frequencies of the fundamental and its first overtone kink ($m = 1$) modes with radial mode number $n = 1$ versus the twist parameter of the annulus, $B_\phi/B_z = \frac{A_0 a}{B_0}$, for different relative core widths $a/R = 0.65$ (dash-dotted), 0.9 (dashed) and 0.99 (solid). The loop parameters are: $L = 10^5$ km, $a/L = 0.01$, $\rho_e/\rho_i = 0.1$, $\rho_0/\rho_i = 0.5$, $\rho_i = 2 \times 10^{-14}$ g cm $^{-3}$, $B_0 = 100$ G. Frequencies are in units of the interior Alfvén frequency, $\omega_{A_i} = 0.02$ rad s $^{-1}$.

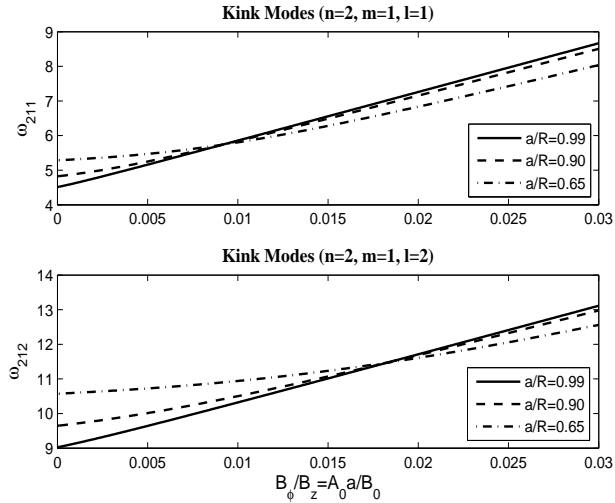


Figure 2: Same as Fig. 1, for the kink ($m = 1$) modes with radial mode number $n = 2$.

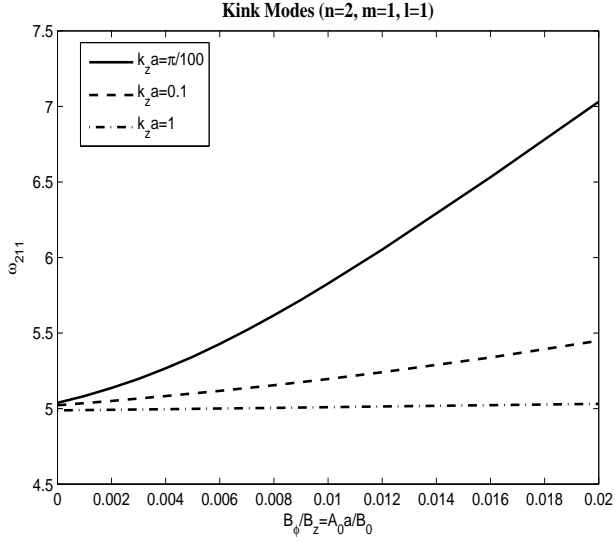


Figure 3: Frequencies of the kink ($m = 1$) modes with radial mode number $n = 2$ versus the twist parameter of the annulus, $B_\phi/B_z = \frac{A_0 a}{B_0}$, for different values of $k_z a = 1$ (dash-dotted), 0.1 (dashed) and $\pi/100$ (solid). Here $a/R = 0.8$ and other auxiliary parameters as in Fig. 1.

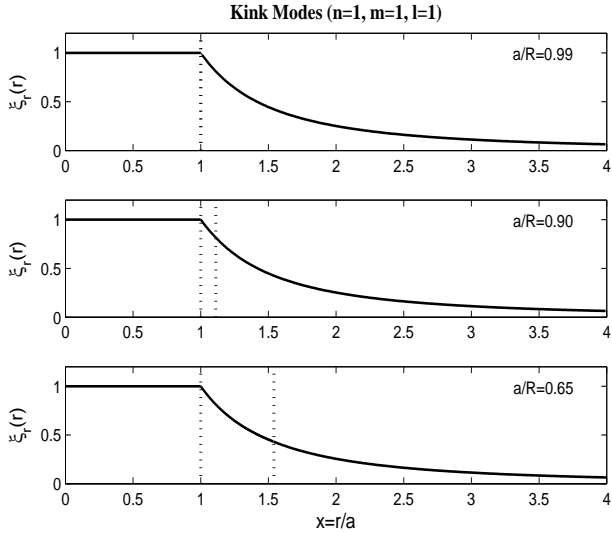


Figure 4: Radial component of the eigenfunctions of the fundamental kink ($m = 1$) modes with radial mode number $n = 1$ against fractional radius $x = r/a$ for $B_\phi/B_z = \frac{A_0 a}{B_0} = 0.0055$ and different relative core widths $a/R = 0.65, 0.9$ and 0.99 .

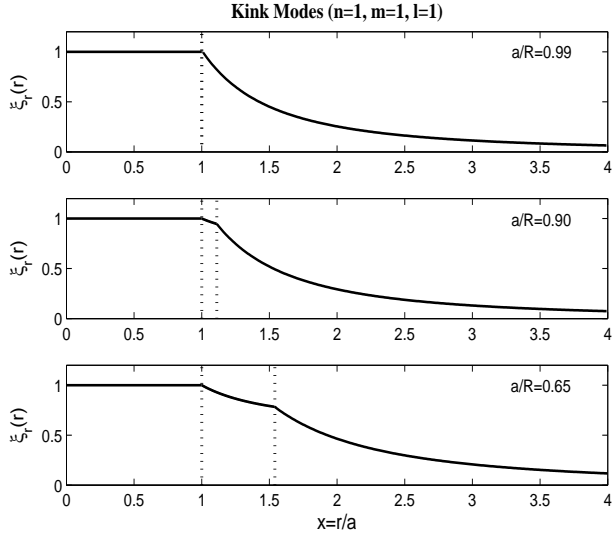


Figure 5: Same as Fig. 4, for $B_\phi/B_z = \frac{A_0 a}{B_0} = 0.02$.

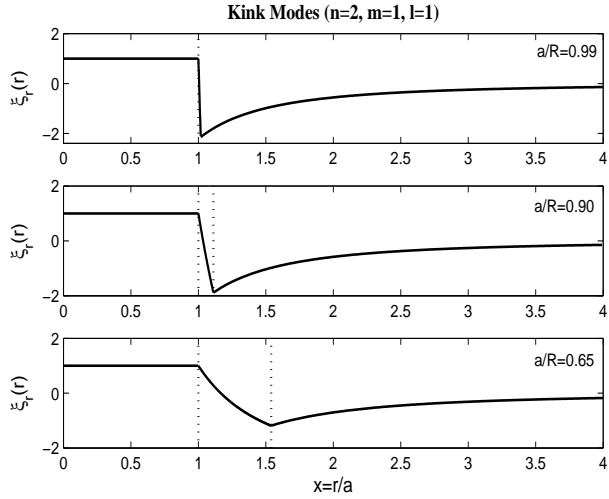


Figure 6: Radial component of the eigenfunctions of the fundamental kink ($m = 1$) modes with radial mode number $n = 2$ against fractional radius $x = r/a$ for $B_\phi/B_z = \frac{A_0 a}{B_0} = 0.02$ and different relative core widths $a/R = 0.65, 0.9$ and 0.99 .

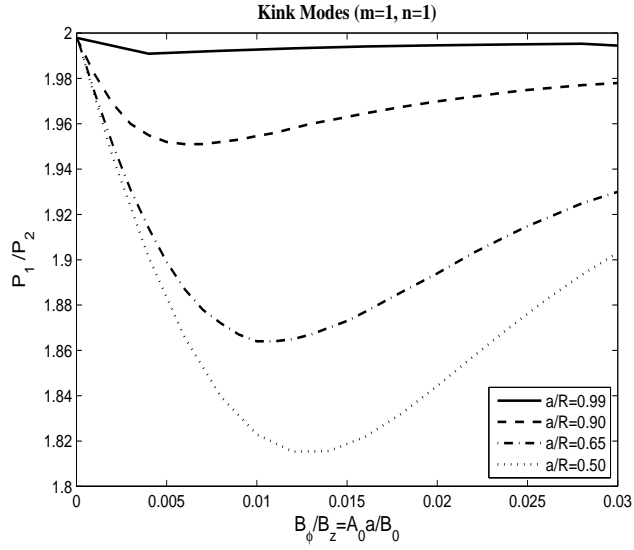


Figure 7: The period ratio P_1/P_2 of the fundamental and its first overtone kink ($m = 1$) modes with radial mode number $n = 1$ versus the twist parameter of the annulus for different relative core widths $a/R = 0.5$ (dotted), 0.65 (dash-dotted), 0.9 (dashed) and 0.99 (solid). Auxiliary parameters as in Fig. 1.

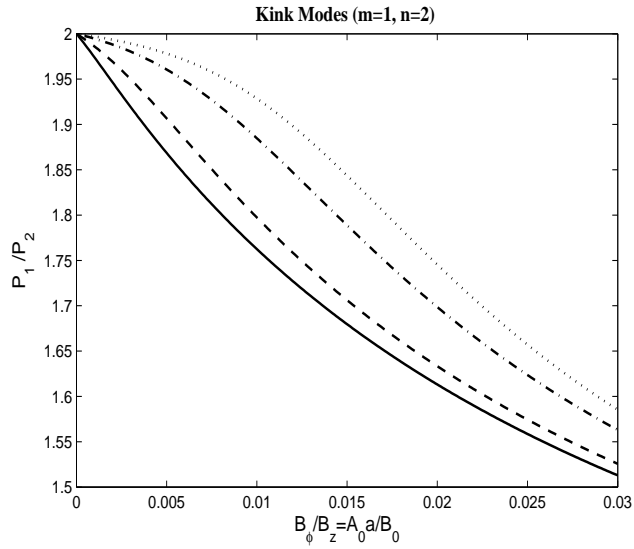


Figure 8: Same as Fig. 7, for the kink ($m = 1$) modes with radial mode number $n = 2$.

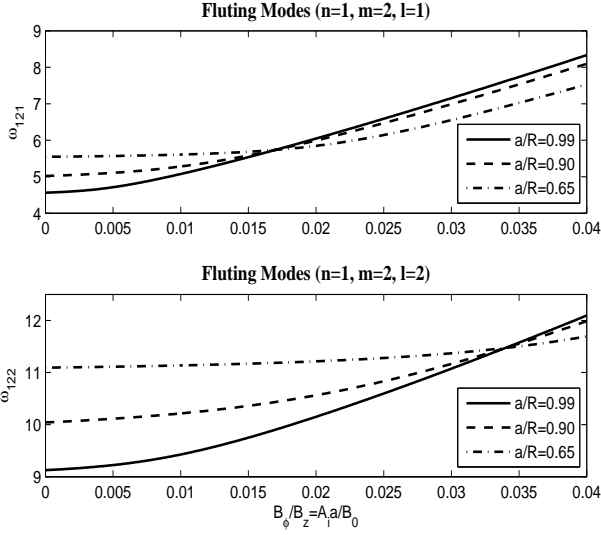


Figure 9: Frequencies of the fundamental and its first overtone fluting ($m = 2$) modes with radial mode number $n = 1$ versus the internal twist parameter, $B_\phi/B_z = \frac{A_i a}{B_0}$, for different relative core widths $a/R = 0.65$ (dash-dotted), 0.9 (dashed) and 0.99 (solid). The twist in the annulus region is absent. Auxiliary parameters as in Fig. 1.

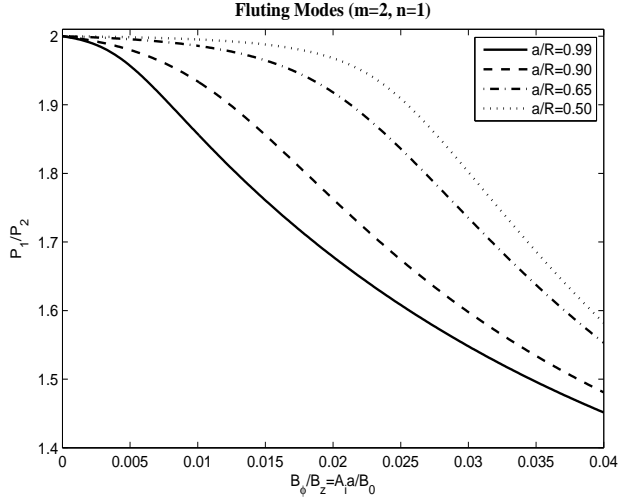


Figure 10: The period ratio P_1/P_2 of the fundamental and its first overtone fluting ($m = 2$) modes with radial mode number $n = 1$ versus the internal twist parameter, $B_\phi/B_z = \frac{A_i a}{B_0}$, for different relative core widths $a/R = 0.5$ (dotted), 0.65 (dash-dotted), 0.9 (dashed) and 0.99 (solid). The twist in the annulus region is absent. Auxiliary parameters as in Fig. 1.

Table 1: Coronal seismology using the period ratio P_1/P_2 of the kink modes ($m = 1, n = 1$): the twist parameter of the annulus $B_\phi/B_z = \frac{A_0 a}{B_0}$ and the relative core width a/R .

	P_1/P_2	$B_\phi/B_z = A_0 a/B_0$	a/R
Van Doorselaere et al. (2007)	1.795 ± 0.051	0.0097, 0.0204	0.35
Van Doorselaere et al. (2009)	1.980 ± 0.002	0.0014, 0.0219	0.92
Ballai et al. (2011)	1.82 ± 0.02	0.0079, 0.0231	0.35